Contact-Safe Reinforcement Learning with ProMP Reparameterization and Energy Awareness

Bingkun Huang¹, Yuhe Gong², Zewen Yang¹, Tianyu Ren¹, Luis Figueredo^{1,2}

Abstract—Reinforcement learning (RL) approaches based on Markov Decision Processes (MDPs) are predominantly applied in the robot joint space, often relying on limited task-specific information and partial awareness of the 3D environment. In contrast, episodic RL has demonstrated advantages over traditional MDP-based methods in terms of trajectory consistency, task awareness, and overall performance in complex robotic tasks. Moreover, traditional step-wise and episodic RL methods often neglect the contact-rich information inherent in task-space manipulation, especially considering the contactsafety and robustness. In this work, contact-rich manipulation tasks are tackled using a task-space, energy-safe framework, where reliable and safe task-space trajectories are generated through the combination of Proximal Policy Optimization (PPO) and movement primitives. Furthermore, an energyaware Cartesian Impedance Controller objective is incorporated within the proposed framework to ensure safe interactions between the robot and the environment. Our experimental results demonstrate that the proposed framework outperforms existing methods in handling tasks on various types of surfaces in 3D environments, achieving high success rates as well as smooth trajectories and energy-safe interactions. The project page is available at https://ppt-rl.github.io

I. Introduction

Contact-rich robotic manipulation imposes stringent requirements on safety, adaptability, and robustness due to its discontinuous dynamics, transient contact forces, and complex energy exchanges. Uncontrolled interaction can lead to instability, excessive forces, or unintended motions, posing risks to both the robot and its environment. Ensuring safe physical interaction therefore requires not only effective regulation of energy flow, but also the ability to generate smooth and adaptable trajectories that remain robust under uncertainty. Traditional model-based motion generation approaches (such as Movement Primitives) rely on accurate models and measurements [1], [2], yet such accuracy is difficult to guarantee in practice, particularly for physical interaction tasks. Reinforcement learning (RL), on the other hand, offers the promise of robustness through data-driven exploration and training, and domain randomization, but often produces non-smooth, stepwise policies and lacks explicit safety guarantees. To address these challenges, several key capabilities are required for a safe smooth manipulation framework, (1) contact-aware representations that capture task-space constraints and uncertainties; (2) trajectory-level planning strategies that ensure smooth, dynamically feasible motions, such as movement primitives; and (3) explicit mechanisms to regulate energy exchange, ensuring interactions

 1Munich Institute of Robotics and Machine Intelligence, Technische Universität München (TUM), Germany. 2School of Computer Science at The University of Nottingham. Corresponding author: Tianyu Ren <tianyu.ren@tum.de>

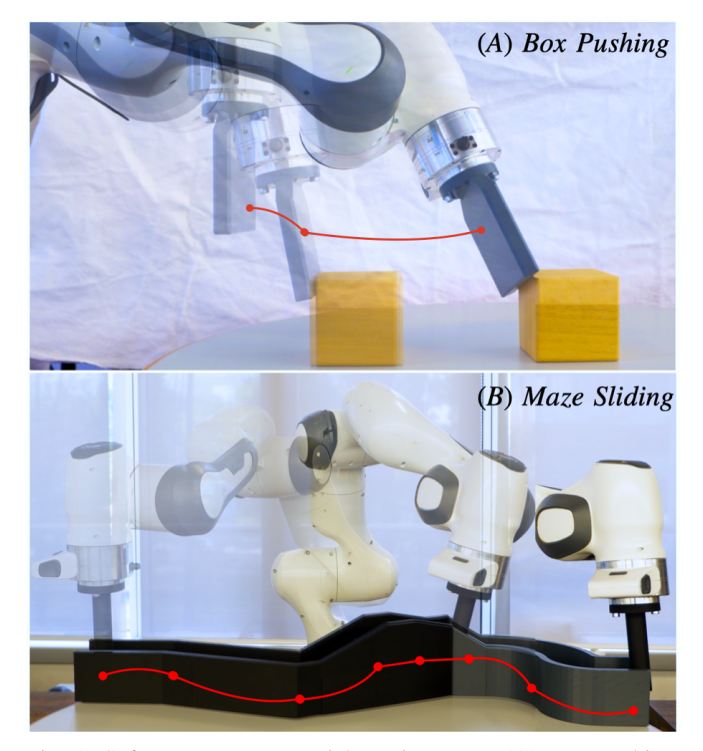


Fig. 1: Safety-aware contact-rich environment. (A) Box pushing: The tool slides along the surface of the block to achieve translation and reorientation. Arrows indicate tangential motion and contact normals, while translucent snapshots illustrate temporal progression. (B) Maze sliding: The tool navigates unseen turns relying solely on contact feedback. Dashed lines represent the executed tool trajectory, and dots mark via-points used to condition the ProMP prior. A 5 cm scale bar is included for reference. This environment requires rich contact information regarding energy to ensure the safe manipulation of the box and navigation within the maze. Excessive energy may lead to damage to either the environment or the robot.

remain within safe operating bounds through passivity-based and energy-aware control. Separately, each of these represents well-developed areas in robot learning and control, however no existing framework combines data-driven robustness, trajectory-level smoothness, and passivity-based safety in contact-rich settings. Indeed, despite being a critical building block to achieve reliable, adaptive, and safe performance in physical manipulation tasks, this integration remains a largely unexplored problem—up to today. This work introduces a novel paradigm that embeds a RL training framework in task-space representation, incorporating awareness of contact-rich information while explicitly ensuring energy-safe interactions.

A. Related Work

Despite the growing success of RL for manipulation [3]–[5], its application to contact-rich tasks remains relatively

limited [6]. Most RL methods are developed and evaluated in joint space or quasi-contact scenarios, where physical interaction with the environment are minimal and forces can be neglected [3], [4]. Contact-rich manipulation, such as pushing, sliding, or assembly, introduces discontinuous dynamics, high-dimensional contact forces, and complex energy exchanges, which pose significant challenges for traditional RL algorithms. Existing work in this area has mainly explored either model-based approaches that incorporate simplified contact dynamics or force feedback into policy learning [7], [8], or *episodic*-RL combined with movement primitives to improve trajectory consistency under contact constraints [9], [10]. However, these approaches are still scarce and often struggle with generalization to unseen contacts, safe energy management, and real-time execution in complex 3D environments.

Building on these limitations, Safe RL [11] aims to enforce safety constraints during both learning and execution, such as limits on peak force, power, or energy. However, in contactrich manipulation, transient forces, frictional uncertainties, and discontinuous dynamics make precise constraint modeling difficult, often limiting SafeRL's effectiveness. As illustrated in Fig. 1, even simple tasks like box pushing or maze sliding involve rich contact interactions where excessive energy could damage the robot or the environment. These scenarios highlight the need for additional mechanisms that explicitly regulate energy representation.

In this context, passivity-based control combined with energy tank frameworks has emerged as a complementary approach for safe contact-rich manipulation. Passivity-based control ensures system stability by preventing the robot from generating uncontrolled energy during physical interactions [12], [13], while energy tanks explicitly monitor and bound the energy exchanged with the environment, enforcing a physically consistent limit on forces and motion [14]. These mechanisms provide a principled foundation for safety in tasks with discontinuous dynamics and high-dimensional contact forces. However, their conservative nature often limits task performance, as purely energy-based passivity constraints do not directly optimize for efficiency, trajectory smoothness, or task-specific objectives.

To address the limitations of both SafeRL and purely passivity-based approaches, RL can in principle be combined with energy-aware controllers and trajectory-level representations, enabling the system to learn task-optimal behaviors while respecting safety constraints in complex, contactrich scenarios. Recent research has explored related aspects from complementary perspectives. To improve trajectory consistency and handle sparse rewards, Otto et al. demonstrated that policies parameterizing movement primitives can generate smoother trajectories compared to low-level stepwise policies [15]. For better generalization to unforeseen geometries or constraints, Zhou et al. proposed via-point movement primitives that enhance trajectory adaptability in novel environments [16]. From a safety standpoint, passivitybased and energy-tank approaches explicitly regulate energy and interaction forces to ensure stability; for example, Zhang et al.'s passivity-centric framework introduces energy constraints to guarantee safe interactions, though it is applied outside of trajectory-level policy learning [17].

Despite these advances, there remains no framework that jointly couples RL with trajectory-level movement primitives and energy-/passivity-aware execution for contactrich manipulation. Such a integration is necessary condition to achieve smooth, task/policy-optimized trajectories under energy constraints that remain smooth and compliant at the point of contact—enabling robust interactions in contact-rich manipulation, which motivates the approach presented in this work. Addressing this gap is important to curb dicey exploration that typically derails learning in contact and enables safe, repeatable behavior on real hardware without task-specific retuning. The impact is a practical path to deployable manipulation policies that generalize across contact conditions while preserving strict energy-safety limits.

B. Contribution

The key novelty of this work lies in integrating reinforcement learning with trajectory-level movement primitives and Cartesian impedance control under energy-aware, passivityenforced constraints for contact-rich manipulation tasks. Rather than relying solely on low-level joint-space RL or stepwise exploration, our framework leverages movement primitives to generate smooth, task-consistent trajectories, while Cartesian impedance control ensures compliant and safe interactions with the environment. These capabilities—readily available in our framework—are often overlooked in prior RL or SafeRL approaches, which either ignore energy safety constraints or do not exploit structured trajectory representations. Similarly, existing passivity-based controllers ensure safety but do not optimize task performance at the trajectory level, leaving a gap between stable, energy-safe control and efficient task execution.

To the best of our knowledge, no prior work has simultaneously combined RL, trajectory-level movement primitives, Cartesian impedance control, and energy-aware passivity constraints in contact-rich manipulation. Our key contributions include, (C1) A task-space RL framework that integrates movement primitives with Cartesian impedance control, enabling the generation of smooth, adaptive, and compliant trajectories for contact-rich manipulation tasks; (C2) A realtime energy-aware passivity controller that enforces force and energy constraints, ensuring safe and robust execution even under discontinuous contact dynamics; (C3) Comprehensive quantitative and real-world evaluations demonstrating that our framework achieves high task success, compliant trajectories, and energy-safe interactions across tasks such as box pushing and maze sliding, outperforming baseline RL and SafeRL methods in both safety and performance.

II. PRELIMINARY

Robotic manipulation in contact-rich environments requires reasoning about trajectories, control forces, and safety simultaneously. In this section, we introduce the core concepts underlying our approach: trajectory representation, reinforcement learning for control adaptation, physical safety via passivity, and impedance-based execution.

A. Trajectory Representation with ProMPs

To model complex trajectories in a compact and adaptable way, we employ Probabilistic Movement Primitives (ProMPs) [18]. ProMPs encode a distribution over trajectories rather than a single deterministic path, allowing the robot to capture variability observed in demonstrations.

Let $\phi \in [0,1]$ denote a canonical phase variable, and $\Phi(\phi) \in \mathbb{R}^{D \times K}$ a set of basis functions (e.g., radial basis functions). A trajectory $y(\phi) \in \mathbb{R}^D$ is expressed as

$$y(\phi) = \Phi(\phi)w, \quad w \sim \mathcal{N}(\mu_w, \Sigma_w),$$
 (1)

where $\boldsymbol{w} \in \mathbb{R}^K$ are the trajectory weights. The Gaussian prior over w captures demonstration variability, while the linear combination ensures smoothness and computational tractability. In our method, we extend ProMPs with viapoint conditioning and reinforcement-learning-based residual updates (Sec. IV).

B. Reinforcement Learning with PPO

While ProMPs provide structured priors, adapting them to new environments or tasks requires learning-based refinement. We model the control problem as a Markov Decision Process (MDP) $\mathcal{M} = (\mathcal{S}, \mathcal{A}, P, r, \gamma)$, where \mathcal{S} is the state space, \mathcal{A} the action space, P the transition dynamics, r the reward function, and γ the discount factor.

A stochastic policy $\pi_{\theta}(a|s)$ outputs a probability distribution over actions given a state. We optimize the policy using Proximal Policy Optimization (PPO) [4], which stabilizes learning by limiting the magnitude of policy updates. The clipped surrogate objective is

$$\mathcal{L}_{\text{clip}}(\theta) = \mathbb{E}_t \left[\min \left(r_t \hat{A}_t, \bar{r}_t \hat{A}_t \right) \right], \tag{2}$$

$$\mathcal{L}_{\text{clip}}(\theta) = \mathbb{E}_t \Big[\min (r_t \hat{A}_t, \bar{r}_t \hat{A}_t) \Big], \qquad (2)$$

$$\bar{r}_t \coloneqq \text{clip}(r_t, 1 - \epsilon, 1 + \epsilon), \quad r_t \coloneqq \frac{\pi_{\theta}(a_t | s_t)}{\pi_{\theta_{\text{old}}}(a_t | s_t)}, \quad (3)$$

where $s_t \in \mathcal{S}$, $a_t \in \mathcal{A}$, \hat{A}_t is the estimated advantage (e.g., via GAE), and ϵ is a small clipping parameter. PPO refines ProMP-generated references to improve task performance while maintaining stable learning.

C. Safety via Passivity and Energy-Tank Mechanisms

When interacting with the environment or humans, safety is critical. We enforce passivity, which ensures that the robot cannot inject unbounded energy [19], [20]. Let $E \in \mathbb{R}_{>0}$ denote the robot's stored energy (kinetic + potential), and $p \in$ \mathbb{R} the instantaneous power exchanged with the environment. Passivity is expressed as

$$\dot{E} < p.$$
 (4)

This constraint prevents high-impact forces, actuator saturation, and instability. Energy-tank mechanisms [21] explicitly enforce this bound, ensuring safe execution of learned or planned trajectories.

D. Cartesian Impedance Control

Finally, to execute trajectories while interacting with the environment, we employ Cartesian impedance control. Let (x_d, R_d) be the desired end-effector pose, with position error $e_x = x_d - x$ and orientation error $e_R = \frac{1}{2} (R_d^{\top} R - R^{\top} R_d)^{\vee}$, where $\boldsymbol{x} \in \mathbb{R}^3$, $\boldsymbol{R} \in SO(3)$, and $(\cdot)^{\vee}$ maps a skew-symmetric matrix to a vector.

A standard Cartesian impedance law is

 $f = K_p e_x + K_d \dot{e}_x, \qquad \tau = K_{p,R} e_R + K_{d,R} \omega_e.$ (5) Here $oldsymbol{f} \in \mathbb{R}^3$ and $oldsymbol{ au} \in \mathbb{R}^3$ are the commanded Cartesian force and torque at the end-effector. The resulting wrench and executed joint torques are

$$m{\lambda} = egin{bmatrix} m{f} \\ m{ au} \end{bmatrix} \in \mathbb{R}^6, \qquad m{ au}_{ ext{imp}} = m{J}^ op(m{q}_t) \, m{\lambda},$$
 where $m{J}(m{q}_t)$ is the $6{ imes}n$ geometric Jacobian, and

 $K_p, K_d, K_{p,R}, K_{d,R}$ are positive-definite gains. This controller executes ProMP- and PPO-generated references while maintaining compliance and safety.

III. PROBLEM DEFINITION

A. Overview of the System

Our framework, PPT (ProMP PPO Energy-Tank), integrates three complementary components: (i) ProMPs for structured, low-dimensional trajectory representation; (ii) **PPO** for adaptive, learning-based trajectory refinement; and (iii) Energy-tank passivity control for safe execution.

The system operates as follows:

- 1) Trajectory Representation: ProMPs encode robot trajectories as distributions over basis functions, allowing smooth and low-dimensional motion representation.
- 2) Policy Refinement: PPO updates the ProMP weights at each timestep,

$$\Delta \mathbf{w}_t = \pi(o_t),\tag{6}$$

to adapt trajectories based on observed performance.

3) Safe Execution: Trajectories generated from ProMP weights,

$$\mathbf{y}_t = \mathbf{\Phi}(\phi_t) \mathbf{w}_t, \tag{7}$$

are updated online according to energy feedback. The energy-tank mechanism ensures interaction forces remain within safe limits.

4) **Online Adaptation:** At test time, partial task-specific constraints can be provided via a small set of via-points

$$D_t = \{ (\phi_i, y_i, \Sigma_i) \}_{i=1}^{N_t}, \tag{8}$$

which are incorporated by a conditioning operator C:

$$\boldsymbol{w}_{t}^{\star} = \mathcal{C}(\boldsymbol{w}_{t}; D_{t}), \quad \boldsymbol{y}_{t} = \Phi(\phi_{t})\boldsymbol{w}_{t}^{\star}.$$
 (9)

This integration allows the system to generate smooth, adaptive trajectories while maintaining safe energy interactions and generalization to unseen environments.

B. Problem Statement.

We consider the problem of learning a policy $\pi_{\theta}(u_t \mid s_t)$ for a robot in a contact-rich environment, where $s_t \in \mathcal{S}$ denotes the robot state and $u_t \in \mathcal{U}$ the control input at time t. The robot interacts with dynamic and partially unknown objects, surfaces, or humans.

The goal is to maximize a cumulative task reward

$$R = \sum_{t=0}^{T} r(s_t, u_t),$$

while ensuring safety and adaptability. The reward encodes four key aspects:

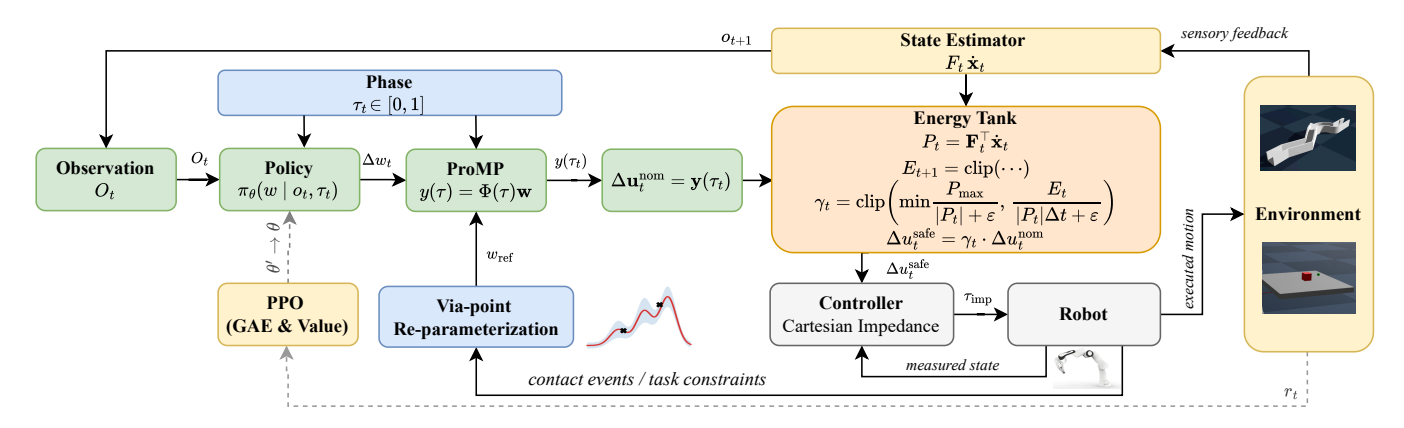


Fig. 2: Overview of the PPT framework. Observations and a phase variable are fed to the policy, which outputs residual ProMP weights. These are combined with via-point conditioned reference weights to form a ProMP trajectory. An energy-tank layer scales the command to ensure safe execution, which a Cartesian impedance controller tracks and converts to joint torques. Interaction feedback informs via-point reparameterization. PPO updates the policy using GAE and a value critic (dashed arrow).

- 1) **Goal / Path Shaping:** encourages progress toward the task goal and proper path following.
- Task Generalization: encourages trajectory adaptation in free space.
- Contact-phase / Haptic Locomotion: ensures safe and effective motion during contact.
- Power / Energy Safety: penalizes excessive forces or energy usage.

Formally, the problem can be expressed as

$$\begin{aligned} \max_{\pi_{\theta}} \quad & \mathbb{E}\left[\sum_{t=0}^{T} r(s_{t}, u_{t})\right] \\ \text{s.t.} \quad & s_{t+1} = f(s_{t}, u_{t}), \quad s_{0} \sim \mathcal{S}_{0}, \quad s_{T} \in \mathcal{S}_{\text{goal}}, \ u_{t} \in \mathcal{U}, \\ & \underbrace{P_{t} = \boldsymbol{\lambda}_{t}^{\text{nom}}^{\top} \boldsymbol{\nu}_{t}, \quad p_{t} := |P_{t}|,}_{\text{instantaneous power (6D)}} \\ & 0 \leq E_{t} \leq E_{\text{max}}, \quad \gamma_{t} \in [0, 1], \\ & \boxed{\gamma_{t} \leq \frac{P_{\text{max}}}{\text{max}(\varepsilon, p_{t})}, \quad \gamma_{t} \leq \frac{E_{t}}{\Delta t \text{ max}(\varepsilon, p_{t})}} \\ & u_{t} = \gamma_{t} \, u_{t}^{\text{nom}}, \quad u_{t}^{\text{nom}} = \pi_{\theta}(o_{t}), \\ & E_{t+1} = \min\{E_{\text{max}}, \quad \max\{0, E_{t} - \gamma_{t} \, p_{t} \, \Delta t\}\}. \end{aligned}$$

where $\pi_{\theta}(u_t \mid s_t)$ is the stochastic policy (params θ), $s_t \in \mathcal{S}$ the robot state, $u_t \in \mathcal{U}$ the executed control, o_t the observation, T the horizon, and $r(s_t, u_t)$ the step reward; the expectation is over rollouts induced by π_{θ} and dynamics $f.\ f: \mathcal{S} \times \mathcal{U} \to \mathcal{S}$ is the system dynamics, \mathcal{S}_0 the initial-state distribution, $\mathcal{S}_{\text{goal}}$ the goal set, and \mathcal{U} the admissible control set. $\lambda_t^{\text{nom}} = [f_t^{\text{nom}}; \tau_t^{\text{nom}}]$ is the nominal 6D wrench, $\nu_t = [\dot{x}_t; \omega_t]$ the 6D twist, $P_t = \lambda_t^{\text{nom}^\top} \nu_t$ the instantaneous power, $p_t := |P_t|$ its magnitude, Δt the control step, $\varepsilon > 0$ a small constant, E_t the energy-tank level (capacity E_{max}), P_{max} the power limit, $\gamma_t \in [0,1]$ the safety scaling factor, $u_t^{\text{nom}} = \pi_{\theta}(o_t)$ the nominal command, and $u_t = \gamma_t u_t^{\text{nom}}$ the safe command. (3D special case: replace λ, ν with f, \dot{x} .)

The objective is to learn a policy that can *generalize to* unseen geometries, produce smooth, compliant trajectories, and maintain energy-safe interactions in contact-rich environ-

ments.

IV. PPT: CONTACT-SAFE RL WITH PROMP

Building upon the preliminaries, our method introduces a task-space reinforcement learning framework that enables *online trajectory adaptation* while explicitly enforcing *energy-safe interactions* in contact-rich tasks. The framework integrates three key components: structured trajectory priors, policy-driven adaptation, and passivity-based safety.

A. Trajectory Prior with ProMP

We represent a d-DoF task-space trajectory using a canonical phase variable $\phi \in [0,1]$ and K radial basis functions (RBFs):

$$y(\phi) = \mathbf{\Phi}(\phi)^{\top} \mathbf{w}, \qquad \Phi_k(\phi) = \exp\left(-\frac{(\phi - c_k)^2}{2\sigma_k^2}\right),$$
 (11)

where $\mathbf{w} \in \mathbb{R}^{K \times d}$ are the basis weights, c_k and σ_k denote the centers and widths of RBF, respectively. We place a Gaussian prior over the vectorized weights:

$$\boldsymbol{w} \sim \mathcal{N}(\boldsymbol{\mu}_w, \boldsymbol{\Sigma}_w),$$
 (12)

with (μ_w, Σ_w) estimated from demonstrations or prior rollouts. This provides a smooth, low-dimensional, and probabilistic trajectory model that captures typical motion patterns while allowing variability.

B. Reinforcement Learning in ProMP Weight Space

Instead of acting directly in the raw control space, the policy refines the ProMP by outputting residual updates in weight space:

$$\mathbf{w}_t = \mathbf{w}_{ref} + \Delta \mathbf{w}_t, \qquad \Delta \mathbf{w}_t \sim \pi_{\theta}(\cdot \mid o_t),$$
 (13)

where o_t includes state, contact information, and the current phase ϕ_t . The adapted weights decode to references

$$\hat{y}_t = \mathbf{\Phi}(\phi_t)^{\top} \mathbf{w}_t$$

which are mapped to Cartesian impedance commands, yielding the nominal control u_t^{nom} . The policy π_{θ} is trained using PPO with the clipped surrogate objective:

$$\mathcal{L}(\theta) = \mathbb{E}_t \left[\min \left(r_t(\theta) \hat{A}_t, \operatorname{clip}(r_t(\theta), 1 - \epsilon, 1 + \epsilon) \hat{A}_t \right) \right], (14)$$

where $r_t(\theta)$ is the likelihood ratio and \hat{A}_t is the advantage estimate. Operating in weight space leverages the structure

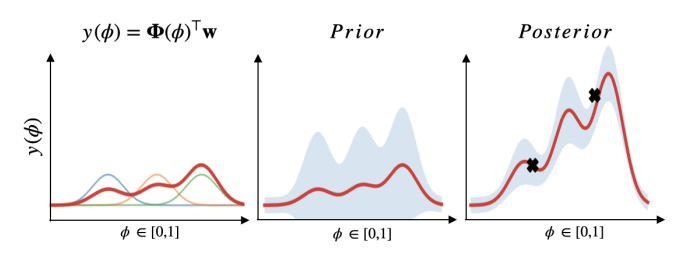


Fig. 3: **ProMP prior and via-point posterior (1D view).** Left: trajectory represented as $y(\phi) = \Phi(\phi)^{\top} \mathbf{w}$ with K RBFs. Middle: prior $\text{vec}(\mathbf{w}) \sim \mathcal{N}(\boldsymbol{\mu}_w, \boldsymbol{\Sigma}_w)$: mean (red) $\pm 2\sigma$ band (blue). Right: posterior conditioned on via-points \mathcal{D} (black \times), showing tightened uncertainty near constraints while preserving smoothness.

and smoothness of ProMPs while enabling online trajectory adaptation.

C. Trajectory Posterior via Via-Point Conditioning

To incorporate partial geometric or contact constraints, we condition the prior on a set of via-points $\mathcal{D} = \{(\phi_j, \mathbf{y}_j)\}_{j=1}^M$ with observation covariance Σ_D . Define

$$\mathbf{H} = egin{bmatrix} \mathbf{\Phi}(\phi_1)^{ op} \ dots \ \mathbf{\Phi}(\phi_M)^{ op} \end{bmatrix}, \quad \mathbf{y}_{\mathcal{D}} = egin{bmatrix} \mathbf{y}_1 \ dots \ \mathbf{y}_M \end{bmatrix}.$$

The posterior distribution over weights is

$$\mathbf{\Sigma}_{w|\mathcal{D}} = (\mathbf{\Sigma}_w^{-1} + \mathbf{H}^{\mathsf{T}} \mathbf{\Sigma}_D^{-1} \mathbf{H})^{-1}, \tag{15}$$

$$\boldsymbol{\mu}_{w|\mathcal{D}} = \boldsymbol{\Sigma}_{w|\mathcal{D}} (\boldsymbol{\Sigma}_{w}^{-1} \boldsymbol{\mu}_{w} + \mathbf{H}^{\top} \boldsymbol{\Sigma}_{D}^{-1} \mathbf{y}_{\mathcal{D}}). \tag{16}$$

The posterior mean $\mu_{w|\mathcal{D}}$ defines a trajectory that interpolates the via-points while preserving smoothness. We set $\mathbf{w}_{\text{ref}} = \text{unvec}(\mu_{w|\mathcal{D}})$ and let PPO learn residual refinements $\Delta \mathbf{w}_t$ on top, effectively separating geometry-constrained adaptation from performance-driven learning.

D. Energy-Tank Layer for Safe Execution

To ensure contact safety and passivity, we integrate an *energy-tank mechanism* that monitors instantaneous power

$$p_t = |\boldsymbol{\lambda}_t^{\mathrm{nom}^{\top}} \boldsymbol{\nu}_t|$$

and scales the nominal control $u_t^{\mathrm{nom}} = \pi_\theta(o_t)$ by a factor $\gamma_t \in [0,1]$. According to the power and energy limits in Eq. (10), the executed command

$$u_t = \gamma_t u_t^{\text{nom}}$$

is constrained by

$$\gamma_t \leq \min\left(\frac{P_{\max}}{\max(\varepsilon, p_t)}, \ \frac{E_t + u_{\text{in}}}{\Delta t \ \max(\varepsilon, p_t)}\right),$$

with limiting $\gamma_t \in [0,1]$ and the control commands $u_t = \gamma_t u_t^{\text{nom}}$, with u_t generating from the policy $u_t^{\text{nom}} = \pi_{\theta}(o_t)$.

Thus, the tank state is updated as

$$E_{t+1} = \min\{E_{\max}, \max\{0, E_t - \gamma_t p_t \Delta t + u_{\text{in}}\}\}.$$

This layer directly scales Cartesian-force commands (extendable to velocity or other channels), ensuring passivity regardless of the policy and stabilizing contact-rich interactions.

V. EXPERIMENTS

We design two complementary experiments to validate our method: (i) a pushing task to highlight the smoothness and stability benefits of ProMP-based trajectory generation, and (ii) a 3D maze sliding task to evaluate the generalization capability when facing unseen surface variations.

Variant	Policy type	Safety layer	Action
PP	Episode-level ProMP	–	ProMP parameters ProMP parameters
PPT	Episode-level ProMP	Energy tank √	
S	Step-wise PPO	–	Cartesian velocity Cartesian velocity
ST	Step-wise PPO	Energy tank √	

TABLE I: Method variants (PPT is our primary method).

A. Common Experimental Setup

- a) Platform and timing: All simulations are conducted in the Genesis physics simulator [22] using a 7-DoF Franka Emika Panda arm. Genesis performs dynamics integration at 2 kHz, while the high-level controller operates at $100\,\mathrm{Hz}$ with a fixed timestep of $\Delta t = 0.01\,\mathrm{s}$. The same controller frequencies are maintained for real-world experiments to ensure consistency between simulation and hardware.
- b) Policy, actions, and tracking.: We train policies using rsl_rl PPO with GAE [23], employing an actor–critic MLP with ReLU activations (256–256–128) and an adaptive learning rate, over 1000 episodes with parallel environments. Two policy parameterizations are considered: (i) episode-level ProMP, which outputs trajectory weights, and (ii) step-wise PPO, which directly outputs Cartesian velocity commands. For the ProMP variants, a Cartesian impedance controller tracks the generated reference trajectories.
- c) Safety constraint (energy tank).: We enforce a power budget through the energy-tank mechanism described in Sec. IV. The instantaneous mechanical power is computed as $P_t = \mathbf{F}_t^{\top} \mathbf{v}_t$ and is constrained by $P_t \leq P_{\max}$. Exceeding this limit incurs a penalty and may result in episode termination. The same power-safety mechanism is applied consistently in both simulation and real-world experiments.
- d) Observations and sensing.: Observations consist of joint positions and velocities, end-effector pose and twist, as well as wrist wrench measurements. On the hardware, we use the Franka external-wrench estimate, while in simulation



Fig. 4: End-effector tools for experiments.

- e) End-effector tools.: Two rigid tools are employed (Fig. 4): a slim paddle $(12 \times 1 \times 1 \text{ cm})$ for the pushing task, and a PLA cylinder (length 12 cm, diameter 2.5 cm) for the maze-sliding task. The physical maze is fabricated via PLA FDM, intentionally leaving a coarse surface finish to increase contact variability, while the simulation imports the exact STL geometry to match the real-world layout.
- f) Training and reporting protocol.: Unless otherwise specified, results are reported as mean \pm SE over k random seeds, with curves smoothed using a moving-average window of w steps. The episode horizon and success criteria are

Metric	Unit	Definition
Max Power	W	Maximum instantaneous powerper episode.
Success rate	%	-
Jerk RMS	m/s^3	End-effector jerk root-mean-square.
Peak wrench (P95)	N	95th percentile of wrench norm P95($\ \mathbf{w}_t\ $).
Overload ratio	%	Time fraction with $P_t > P_{\text{max}}$.
Contact continuity	0-1	Mean duration/ratio of contact segments.
Progress@T	0-1	Normalized progress at horizon T .

TABLE II: Evaluation metrics shared by all experiments; taskspecific thresholds/horizons are defined in each subsection.

task-specific and detailed in the corresponding subsections. Domain randomization is applied within task-dependent ranges (e.g., friction, mass)

B. Simulation Experiments

1) Box Pushing: A slim paddle is used to push a box across a planar tabletop from a designated start region to a goal. Task-specific domain randomization is applied on a per-episode basis: the kinetic friction coefficient is sampled as $\mu_k \sim \mathcal{U}(0.20, 0.60)$ (with static friction $\mu_s = 1.25\,\mu_k$), and the box mass is jittered by $\pm 15\%$ around two nominal sizes (6 cm / 50 g and 8 cm / 80 g). During training, the policy has access to privileged box pose information for faster credit assignment; at test time, this information is removed, leaving only start and goal positions (partial observability).

Across random seeds (Fig. 5), the ProMP-based trajectory policy with energy tank (PPT) exhibits rapid and steady learning, reaching a high success plateau while maintaining the lowest near-peak power. The energy tank effectively clamps force bursts during exploratory contact. The stepwise variant with the same safety layer (ST) converges more slowly and shows higher variance due to per-step action fluctuations. A step-wise policy without the tank (PP) learns quickly but suffers occasional regressions, while the step-wise baseline without safety (S) is the least stable. Although heavier

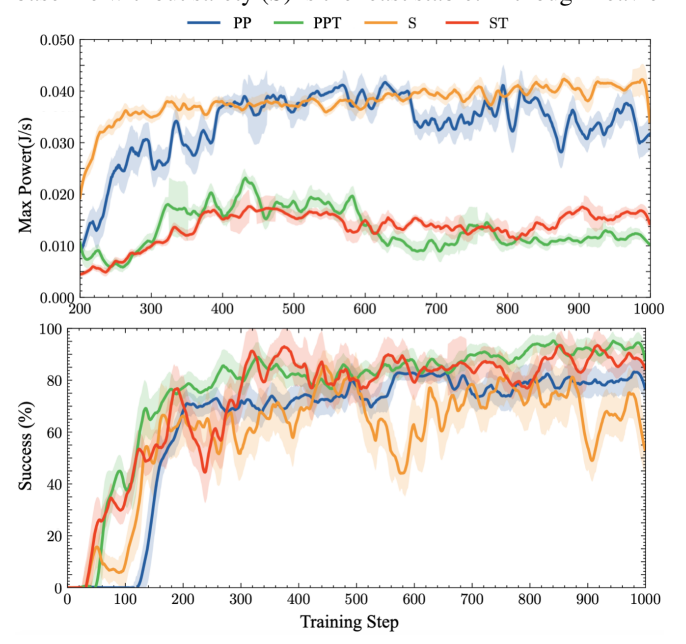


Fig. 5: **Training curves.** Success rate (%) and max instantaneous power (W) vs. training steps for **PP**, **PPT**, **S**, **ST**. Higher success and lower power are better.





Fig. 6: Maze sliding scenarios. Left: training on straight corridors to learn a phase-aligned wall-following prior. Right: deployment in an unseen maze with turns, a disc-like segment, and height variations.

boxes increase absolute task difficulty, the relative ordering among methods is preserved, demonstrating that trajectorylevel generation combined with energy shaping mitigates violent exploration and enhances reliability in contact-rich interactions.

2) Maze Sliding: Policies are trained exclusively in straight corridors to acquire a phase-aligned wall-following prior, and are subsequently deployed in unseen mazes (corridor width 5–6 cm, total length ~ 1 m) featuring $20^{\circ}-45^{\circ}$ turns, a disc-shaped segment, and up to 4 cm vertical undulations. Observations are limited to proprioception and wrist wrench measurements (no map or vision). Domain randomization includes variations in start pose, heading, and bounded wall friction. The power budget follows the standard setup, and the episode horizon is $T=20\,\mathrm{s}$.

To isolate the effect of trajectory parameterization, we compare only the deployable, safety-layered variants under the same power budget: PPT and ST. Reward components follow the definitions in Sec. V-A. While PPT requires no task-specific redesign, ST achieves consistent performance only after introducing stronger slip and heading regularization.

Figure 7 demonstrates that the wall-following prior learned in straight corridors successfully transfers to curved and height-varying mazes. Waypoints concentrate near bends, and PPT produces a narrow posterior band that closely adheres to the wall, exhibiting smoother cornering and reduced lateral spread.

Quantitatively (Table III), PPT achieves higher task success and maintains a tighter safety envelope, with lower jerk, reduced near-peak wrench, fewer overload events, and significantly higher contact continuity. In contrast, ST attains slightly higher Progress@T within the fixed horizon. This relative ordering persists across maze layouts and vertical undulations, and PT requires no reward retuning.

Overall, these results highlight that trajectory-level parameterization combined with energy-aware power gating is crucial for safe, contact-only navigation and effective generalization to novel geometries.

C. Real-World Experiments

1) Box Pushing: We evaluate two cubic boxes (edge lengths 6 cm and 8 cm; nominal masses 50 g and 80 g) on a flat laminate tabletop. Surface micro-roughness and dust naturally induce variability in friction and stick-slip behavior, which is *not* explicitly modeled. The energy tank remains active with the same budget as in simulation. Each trial begins

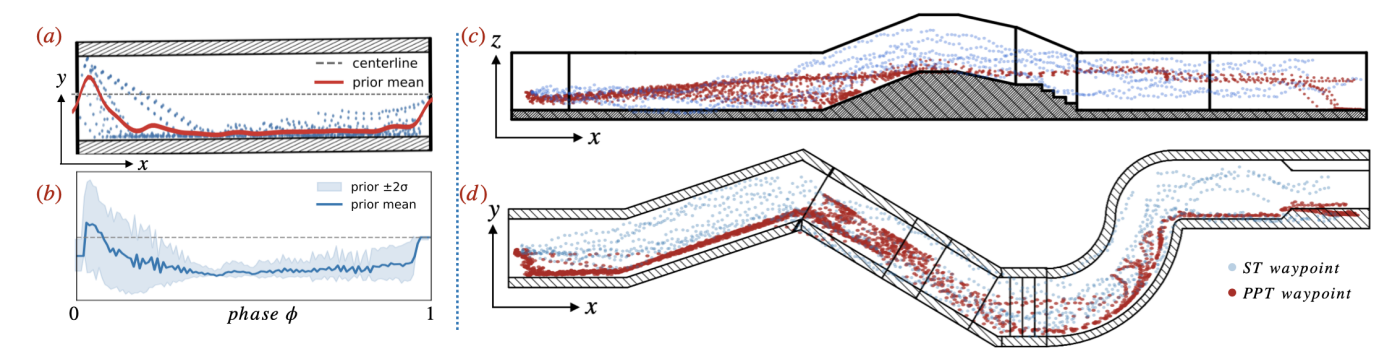


Fig. 7: Maze sliding—training prior and test posterior rollouts (PPT vs. ST). (a) Prior learned on straight corridors: dashed gray centerline and the learned prior mean (solid). (b) Prior dispersion over phase ϕ : mean with $\pm 2\sigma$ band. (c) Test maze in (x-z) view: posterior rollouts with contact-inferred waypoints; PPT in red and ST in blue (dots mark detected waypoints). (d) Same as (c) in (x-y) view. Waypoints cluster near bends/junctions; PPT shows a tighter band and smoother transitions than ST.

from a randomized start pose within a fixed start region and terminates upon goal capture or safety violation.

to the simulation setup.

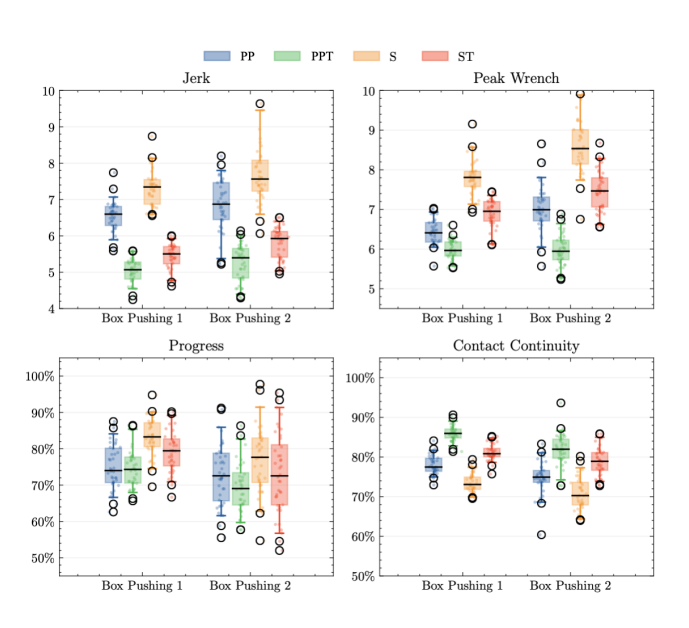


Fig. 8: **Real-world pushing metrics.** Jerk RMS, Peak Wrench P95 (N), Progress (%), and Contact Continuity (%) for two object conditions (*Box Pushing 1/2*). Boxes/whiskers show episode/seed distributions.

PPT consistently yields the lowest jerk and near-peak wrench and the highest contact continuity, indicating smoother motions and steadier contact under the same power budget (Fig. 8). S/ST can reach slightly higher Progress@T on some trials, but at the cost of larger dispersion and more near-overload events, mirroring simulation. Absolute jerk/wrench are modestly higher than in sim due to sensing noise and real stick—slip, but the method ranking is preserved, supporting the robustness of trajectory-level parameterization plus power gating.

2) Maze Sliding: We deploy a 1 m-long PLA maze with corridor widths of 5–6 cm, printed with a deliberately coarse surface finish to enhance contact variability. The maze layout includes 20° – 45° turns, a disc-like segment, and vertical undulations of up to 4 cm. The end-effector is a PLA cylinder, and sensing, filtering, and the energy-tank budget are identical

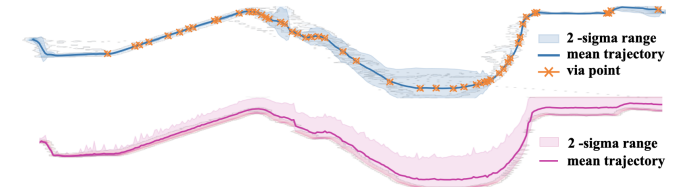


Fig. 9: **Real-world maze sliding.** Top: **PPT**; bottom: **ST**. Trajectory mean and $\pm 2\sigma$ bands are overlaid; dots denote contact-inferred waypoints. Waypoints cluster near bends/junctions; **PPT** shows tighter bands and smoother redirection through corners.

Figure 9 and Table III demonstrate that PPT successfully transfers the straight-corridor prior to complex maze geometries, producing trajectories with tighter dispersion and smoother cornering. It achieves higher task success and a stronger safety envelope, reflected in lower jerk, reduced near-peak wrench, fewer overload events, and higher contact continuity. ST attains slightly higher progress within a fixed horizon (Progress@T) but exhibits larger lateral spread and more frequent near-overload behaviors. Qualitative observations show that contact-inferred waypoints densify around bends; PPT tracks these transitions with minimal overshoot, whereas ST often oscillates before settling. Overall, the simreal trends are consistent: trajectory-level parameterization combined with power gating is key to safe, contact-only navigation, while step-wise control trades stability and safety for speed.

Across both tasks, real-world results corroborate the simulation findings: (i) the energy tank reliably enforces the power budget under unmodeled friction and sensor noise, and (ii) ProMP-based trajectory parameterization yields smoother,

Metric	Unit	PPT	ST
Success rate	%	89	60
Jerk RMS	m/s^3	1.85	2.70
Peak wrench (P95)	N	8.5	11.2
Overload ratio	%	2.3	3.1
Contact continuity	0-1	0.74	0.48
Progress@T	0-1	0.70	0.76

TABLE III: Real-world maze sliding under the same power budget: PPT vs. ST (means).

more stable behavior with higher success. Residual sim-to-real differences, such as slightly higher jerk or wrench, are attributable to measurement noise and surface stick-slip. Notably, PPT required no reward redesign or policy finetuning.

D. Discussion

Our experiments consistently show that the PPT outperforms step-wise policies ST in terms of smoothness and stability. The structured nature of ProMPs promotes globally coherent trajectories, resulting in lower jerk, reduced peak wrench, and higher contact continuity. This inherent smoothness mitigates high-frequency, reactive actions that often destabilize step-wise methods during contact.

The results further highlight the synergy between ProMP-based policies and the energy-tank safety layer. For PPT, the energy tank acts as a robust safety net for unexpected events, whereas for the more erratic ST policy, frequent tank interventions produce hesitant and inefficient motions, compromising performance despite ensuring safety.

Finally, the framework demonstrates strong practical utility, with robust sim-to-real transfer and generalization to unseen maze geometries without policy finetuning. The system effectively handles unmodeled friction and sensor noise, confirming that structured trajectory learning integrated with energy-aware safety is a powerful paradigm for reliable and safe contact-rich manipulation.

VI. CONCLUSION

We present a contact-safe reinforcement learning framework that integrates ProMP-based trajectory learning with a passivity-based energy tank. By combining the smooth, structured, and adaptive policies of ProMPs with the strong safety guarantees of the energy tank, our approach enables stable and efficient contact-rich manipulation across a variety of contact surfaces. Numerical simulations and real-world experiments demonstrate that our method outperforms stepwise RL baselines, achieving higher success rates and smoother, safer interactions with robust sim-to-real transfer. Despite these advantages, our method has limitations. The fixed-budget energy tank can be conservative, potentially limiting task performance, and effective generalization relies on a suitable trajectory prior. Future work will explore adaptive energy management strategies to better balance safety and performance, as well as hierarchical trajectory priors to enhance generalization across a broader range of tasks.

REFERENCES

- B. Armstrong-Hélouvry, P. Dupont, and C. C. de Wit, "A survey of models, analysis tools and compensation methods for the control of machines with friction," *Automatica*, vol. 30, no. 7, 1994.
- [2] M. Jean, "The non-smooth contact dynamics method," Computer Methods in Applied Mechanics and Engineering, vol. 177, no. 3-4, pp. 235–257, 1999.
- [3] T. P. Lillicrap, J. J. Hunt, A. Pritzel, N. Heess, T. Erez, Y. Tassa, D. Silver, and D. Wierstra, "Continuous control with deep reinforcement learning," arXiv:1509.02971, 2015.
- [4] J. Schulman, F. Wolski, P. Dhariwal, A. Radford, and O. Klimov, "Proximal policy optimization algorithms," arXiv preprint arXiv:1707.06347, 2017. [Online]. Available: https://arxiv.org/abs/1707.06347
- [5] S. Levine, C. Finn, T. Darrell, and P. Abbeel, "End-to-end training of deep visuomotor policies," *JMLR*, vol. 17, no. 39, pp. 1–40, 2016.

- [6] J. Kober, J. A. Bagnell, and J. Peters, "Reinforcement learning in robotics: A survey," *The International Journal of Robotics Research*, vol. 32, no. 11, pp. 1238–1274, 2013.
- [7] P. Kormushev, S. Calinon, and D. G. Caldwell, "Reinforcement learning in robotics: Applications and real-world challenges," *Robotics*, vol. 2, no. 3, pp. 122–148, 2013.
- [8] P. Pastor, H. Hoffmann, T. Asfour, and S. Schaal, "From dynamic movement primitives to associative skill memories," *Robotics and Autonomous Systems*, vol. 61, no. 4, pp. 351–361, 2013.
- [9] A. Rajeswaran, V. Kumar, A. Gupta, G. Vezzani, J. Schulman, E. Todorov, and S. Levine, "Learning complex dexterous manipulation with deep reinforcement learning and demonstrations," in RSS, 2018.
- [10] F. Otto, O. Celik, H. Zhou, H. Žiesche, V. A. Ngo, and G. Neumann, "Deep black-box reinforcement learning with movement primitives," in CoRL, 2023.
- [11] J. García and F. Fernández, "A comprehensive survey on safe reinforcement learning," *Journal of Machine Learning Research*, vol. 16, no. 1, pp. 1437–1480, 2015. [Online]. Available: https://www.jmlr.org/papers/volume16/garcia15a/garcia15a.pdf
- [12] R. Ortega, A. van der Schaft, I. Mareels, and B. Maschke, "Passivity-based control of euler-lagrange systems: A survey of some results," *Automatica*, vol. 38, no. 4, pp. 585–596, 2002.
- [13] S. Haddadin and E. Croft, "Physical human-robot interaction," in Springer Handbook of Robotics (2nd ed.), B. Siciliano and O. Khatib, Eds. Cham: Springer, 2016, pp. 1835–1874, often cited as a core reference for safety/pHRI.
- [14] F. Ferraguti, N. Preda, A. Manurung, C. Secchi, and C. Fantuzzi, "An energy tank-based interactive control architecture for autonomous and teleoperated robotic surgery," *IEEE Transactions on Robotics*, vol. 31, no. 5, pp. 1073–1088, 2015.
- [15] F. Otto, O. Celik, H. Zhou, H. Ziesche, V. A. Ngo, and G. Neumann, "Deep black-box reinforcement learning with movement primitives," in *Proceedings of The 6th Conference on Robot Learning*, ser. Proceedings of Machine Learning Research, K. Liu, D. Kulic, and J. Ichnowski, Eds., vol. 205. PMLR, 14–18 Dec 2023, pp. 1244–1265. [Online]. Available: https://proceedings.mlr.press/v205/otto23a.html
- [16] Y. Zhou, J. Gao, and T. Asfour, "Learning via-point movement primitives with inter- and extrapolation capabilities," in 2019 IEEE/RSJ International Conference on Intelligent Robots and Systems (IROS), 2019, pp. 4301–4308.
- [17] H. Zhang, G. Solak, S. Hjorth, and A. Ajoudani, "Passivity-centric safe reinforcement learning for contact-rich robotic tasks," arXiv preprint arXiv:2503.00287, 2025. [Online]. Available: https://arxiv.org/abs/2503.00287
- [18] A. Paraschos, C. Daniel, J. Peters, and G. Neumann, "Probabilistic movement primitives," in *Advances in Neural Information Processing Systems (NeurIPS)*, 2013. [Online]. Available: https://papers.nips.cc/ paper/5177-probabilistic-movement-primitives
- [19] N. Hogan, "Impedance control: An approach to manipulation, part i—theory," *Journal of Dynamic Systems, Measurement, and Control*, vol. 107, no. 1, pp. 1–7, 1985.
- [20] R. Ortega, A. Loria, P. J. Nicklasson, and H. Sira-Ramírez, Passivity-Based Control of Euler-Lagrange Systems: Mechanical, Electrical and Electromechanical Applications, ser. Communications and Control Engineering. London: Springer, 2001.
- [21] S. Haddadin, A. Albu-Schäffer, and G. Hirzinger, "Safety evaluation of physical human–robot interaction via energy-based, ergonomic and dynamic criteria," *The International Journal of Robotics Research*, vol. 31, no. 13, pp. 1578–1595, 2012.
- [22] G. Authors, "Genesis: A generative and universal physics engine for robotics and beyond," December 2024. [Online]. Available: https://github.com/Genesis-Embodied-AI/Genesis
- [23] N. Rudin, D. Hoeller, P. Reist, and M. Hutter, "Learning to walk in minutes using massively parallel deep reinforcement learning," in Proceedings of the 5th Conference on Robot Learning, ser. Proceedings of Machine Learning Research, vol. 164. PMLR, 2022, pp. 91–100. [Online]. Available: https://proceedings.mlr.press/v164/rudin22a.html